Archives of Toxicology
https://doi.org/10.1007/s00204-020-02694-6

NANOTOXICOLOGY

Small silica nanoparticles transiently modulate the intestinal permeability by actin cytoskeleton disruption in both Caco-2 and Caco-2/HT29-MTX models

Raphaël Cornu[1] · Claire Chrétien[1] · Yann Pellequer[1] · Hélène Martin[1] · Arnaud Béduneau[1]

Received: 15 November 2019 / Accepted: 2 March 2020

Abstract
Amorphous silica nanoparticles are widely used as pharmaceutical excipients and food additive (E551). Despite the potential human health risks of mineral nanoparticles, very few data regarding their oral toxicity are currently available. This study aims to evaluate and to understand the interactions of silica particles at 1 and 10 mg mL^{-1} with the intestinal barrier using a Caco-2 monolayer and a Caco-2/HT29-MTX co-culture. A size- and concentration-dependent reversible increase of the paracellular permeability is identified after a short-term exposure to silica nanoparticles. Nanoparticles of 30 nm induce the highest transepithelial electrical resistance drop whereas no effect is observed with 200 nm particles. Additive E551 affect the Caco-2 monolayer permeability. Mucus layer reduces the permeability modulation by limiting the cellular uptake of silica. After nanoparticle exposure, tight junction expression including Zonula occludens 1 (ZO-1) and Claudin 2 is not affected, whereas the actin cytoskeleton disruption of enterocytes and the widening of ZO-1 staining bands are observed. A complete permeability recovery is concomitant with the de novo filament actin assembly and the reduction of ZO-1 bands. These findings suggest the paracellular modulation by small silica particles is directly correlated to the alteration of the ZO-actin binding strongly involved in the stability of the tight junction network.

Keywords Silica nanoparticles · Intestinal permeability · Actin cytoskeleton · Tight junctions · Caco-2 cells

Introduction

Amorphous silica nanoparticles (NPs) represent one of the most common manufactured nanomaterial. Their unique physicochemical properties such as the surface area and the porosity, their great stability and their low cost confer them a major importance in various application fields including pharmaceutical and food industries (Zhou et al. 2018; He et al. 2019). Silica NPs are used as flow agent in the preparation of solid dosage forms and as anti-caking agent in many powdered foods due to their hygroscopic characteristics (Pradhan et al. 2015). Food additive E551 is a mixture of silica NPs with a diameter inferior to 100 nm and microparticles (Barahona et al. 2016; EFSA Panel on Food Additivies and Nutrient Sources added to Food (ANS) et al. 2018). Spherical silica nanoparticles of approximately 10–50 nm in size were clearly identified in food (Athinarayanan et al. 2014). The nanoparticle/microparticle ratio is often different according to the manufacturer.

The use of nanomaterials is more and more questioned due to their potential toxicity in Humans (Jackson et al. 2017; Sahu and Hayes 2017). Recent findings emphasized the potential human health risk induced by food additives composed of nanoparticles. Many scientific studies focused on the additive E171 composed of titanium dioxide (TiO_2) NPs. In vitro and in vivo studies showed that TiO_2 NPs impaired tight junctions and led to an increase of the intestinal permeability (Brun et al. 2014; Pedata et al. 2019). However, very few data regarding the oral toxicity of the additive E551 are available. Concentration-dependent cytotoxicity and oxidative stress caused by the silica NPs were mainly reported (Athinarayanan et al. 2014). However, their effects on the function and the integrity of the intestinal barrier are little studied. A disruption of the intestinal barrier or an increase of the epithelial permeability could

Hélène Martin and Arnaud Béduneau contributed equally to this work.

✉ Arnaud Béduneau
arnaud.beduneau@univ-fcomte.fr

[1] PEPITE EA4267, FHU Increase, Univ. Bourgogne Franche-Comté, 25000 Besançon, France

Published online: 11 March 2020

facilitate the transport of toxic agents, modify the bioavailability of drugs and allow the bacterial translocation (Vancamelbeke and Vermeire 2017). A recent study published by Liu et al. (2017). reported a dysfunction of the blood–brain barrier by silica NPs, demonstrating the potential toxic effect of the silica on the biological barriers.

In the present study, the oral toxicity of the additive E551 and silica nanoparticles with sizes ranging from 10 to 200 nm was investigated. Two in vitro models of the intestinal barrier were compared: a Caco-2 monolayer, considered as the gold standard for predicting intestinal absorption of drugs and a co-culture Caco-2/HT29-MTX. Caco-2 is a human colon carcinoma cell line, exhibiting a phenotype similar to the enterocytes of small intestine. HT29-MTX is a sub-population of human carcinoma cell-lines HT29 isolated by treatment with methotrexate. HT29-MTX plays the role of goblet cells in the co-culture to consider the protective mucus barrier in the toxicity studies. After exposure of NPs to in vitro models of intestinal barrier, the oxidative stress, the inflammatory response and the paracellular permeability were evaluated. The influence of the NP size, the presence of mucus and the intracellular mechanisms involved in the nanotoxicity were also discussed through molecular biology and immunostaining experiments.

Materials and methods

Chemicals and reagents

Silica NPs (plain Sicastar®) and fluorescent silica NPs (Sicastar®-F) were purchased from Micromod Partikeltechnologie GmbH (Rostock, Germany). A red fluorescent dye with excitation and emission wavelengths of 569 nm and 585 nm was covalently bounded to the silica matrix. Additive E551 was provided by Merck Millipore (EMPROVE® ESSENTIAL Ph Eur,NF,JP,E 551). Caco-2 cells were provided by the American Type Culture Collection (ATCC) at passage 47 and HT29-MTX cell line was kindly provided by Dr. Thécla Lesuffleur from INSERM UMR S 938 in Paris, France, at passage 13. All the cell culture reagents were purchased from Fisher Scientific (Illkirch, France). Other chemicals used in our experiments were from Sigma Aldrich (Steinheim, Germany), unless stated otherwise. A transport buffer (TB) consisting in 25 mM D-(+)-glucose, 10 mM HEPES in Hank's Balanced Salt Solution with Ca^{2+} and Mg^{2+} pH 7.4 was used for all experiments.

Physicochemical characterization of silica nanoparticles

Size and zeta potential of silica nanoparticles were characterized using a ZetaSizer Nano-ZS90 (Malvern). Average hydrodynamic diameters and polydispersity index (PDI) were determined by dynamic light scattering at 25 °C after dilutions in TB. Zeta potential measurements were performed by laser Doppler electrophoresis at 25 °C at a final concentration of 1 mg mL^{-1}.

Physical stability of silica NPs in culture medium

The physical stability of NPs was assessed at 37 °C in TB. NP suspensions at a concentration of 1 mg mL^{-1} were prepared. Hydrodynamic diameters, PDI and zeta potential were measured before and after 2-h incubation.

Caco-2/HT29-MTX co-culture in Transwell®

Caco-2 and HT29-MTX cells were cultivated in 25 cm^2 flasks during 2 passages after thawing in Dulbecco's Modified Eagle Medium Gluta-Max containing 15% fetal bovine serum, 1% non-essential amino-acids and 100 µg mL^{-1} streptomycin/100 UI mL^{-1} penicillin. Cells were then cultured in Transwell®-24 well 0.33 cm^2 permeable support with a polycarbonate membrane. Caco-2 cells were seeded at day 0 at 5000 cells per insert and HT29-MTX were seeded at day 5 at 10,000 cells per insert. The Transwell® supports were used at day 21.

Cytotoxic assay

MTT assay

The evaluation of the cell viability was assessed using the 3-(4,5-dimethylthiazol-2-yl)-2,5-diphenyltetrazolium bromide (MTT) method. Cell cultures in Transwell® support were incubated with NPs at 1 and 10 mg mL^{-1} for 2 h. Cells were washed twice with phosphate-buffered saline (PBS) and incubated with MTT (0.5 mg mL^{-1}) for 2 h at 37 °C. The formazan crystals were then dissolved in DMSO. The supernatants were transferred in a 96-well plate and the absorbance was measured at 570 nm with a microplate reader (Synergy HT BioTek).

Lactate dehydrogenase (LDH) assay

The cytotoxicity of silica NPs was also determined using the Pierce LDH cytotoxicity assay kit (ThermoScientific). Briefly, cells in Transwell® support were incubated for 2 h with silica NPs and the apical and basolateral media were collected. Fifty microliters of substrate LDH mixture was added to 50 µL medium and incubated 30 min at room temperature. The absorbance was measured at 490 nm and 680 nm with a microplate reader (Synergy HT BioTek). The percentage of cytotoxicity corresponds to the total percentage of LDH. It was calculated by comparing the LDH

activity of cells treated with NPs and the maximum LDH activity control obtained after addition of a lysis buffer.

Permeability studies

Transepithelial electrical resistance (TEER)

TEER measurement was carried out before and after 2 h incubation with NPs using the Millicell Electrical Resistance System (Millipore). For TEER recovery monitoring, cells were washed twice with PBS after 2 h of incubation and TB containing NPs or Cytochalasin B (Cyt B) (20 µg mL^{-1}) was replaced by fresh complete medium culture. The TEER was then monitored for 22 h at different time points.

Paracellular permeability

After incubation of the Caco-2 monolayer and the co-culture with NPs, Lucifer-Yellow (LY) was added at a concentration of 50 µg mL^{-1} in the apical compartment. After 2 h incubation, the LY concentration in the acceptor compartment was then assessed by fluorescence. $\lambda_{excitation}$ and $\lambda_{emission}$ were 405 nm and 535 nm, respectively. The apparent permeability of LY was then calculated according to the following Eq. (1)

$$P_{app} = \frac{\frac{dQ}{dt}}{A \times C_0}, \quad (1)$$

dQ/dt is the flux with Q, the amount of molecules transported over time t of the incubation, A is the surface area of the polycarbonate membrane (0.33 cm^2), and C_0 is the initial concentration in the donor compartment.

Uptake of silica NPs

Cells in Transwell® insert were incubated 2 h at 37 °C or 4 °C with fluorescent silica NPs at 1 mg mL^{-1}. Caco-2 cells were washed three times with PBS and then lysed with NaOH 0.1 N. Samples were transferred in black 96-well plate. Fluorescence was immediately measured using a microplate reader. $\lambda_{excitation}$ and $\lambda_{emission}$ were 569 nm and 585 nm, respectively. In parallel, for each size of fluorescent NPs, a standard curve was prepared by successive dilutions of NPs in NaOH 0.1 N. Fluorescence signal in cell lysate was compared to standard curves to assess the NP concentration in cells. Then, the percentage of NPs uptake was calculated by comparison with the initial quantity of NPs.

ROS production

The reactive oxygen species (ROS) production was assessed using the ROS-Glo H_2O_2 assay kit (Promega). In brief, cells were incubated 2 h with NPs or H_2O_2 Reagent in the apical compartment. The supernatant was collected and incubated for 20 min at room temperature with ROS-Glo detection solution. The relative luminescence was then recorded.

Cytokine production

The levels of interleukin (IL)-6 and IL-8 were assessed in pooled apical and basolateral supernatants. IL-6 human ELISA high sensitivity kit and IL-8 human ELISA kit (Life Technologies-ThermoFisher) were used according to the manufacturer's instruction. Protein concentrations were determined by Micro BCA Protein Assay (ThermoScientific).

Western blotting

For western blotting analysis, Caco-2 were incubated with NPs during 2 h, washed three times with PBS, and then lysed on ice in RIPA lysis buffer. Lysed samples were centrifuged at 20,000*g* at 4 °C for 15 min. Proteins were quantified by Micro BCA assay, separated on a 12.5% polyacrylamide gel and transferred on a PVDF membrane. Membranes were blocked in 5% nonfat milk in TBS-Tween 0.1% during 1 h, and then incubated with primary antibodies [1:1000 for ZO-1 (Abcam ab216880) and 1:1000 for Claudin 2 (Abcam ab53032)] overnight at 4 °C. This was followed by a 1 h-incubation with secondary antibodies HRP goat anti Rabbit (1:1000) (BD Biosciences 554021). Blots were washed three times in PBS-Tween 0.1% after the incubations with primary and secondary antibodies. Bands were detected using Clarity™ Western ECL and quantified with Image Lab software (BioRad).

Fluorescent staining

Immunostaining of ZO-1

After 2 h incubation with NPs, Caco-2 cells in Transwell® support were washed twice with PBS and then fixed with cold methanol during 5 min. Blocking buffer containing 1% BSA and 22.5 mg mL^{-1} glycine in PBS-Tween 0.1% was added to Caco-2 cells during 30 min. ZO-1 protein was labelled with Rabbit anti-ZO1 tight junction protein antibody (Abcam ab216880) at 5 µg mL^{-1} during 1 h at room temperature in humid chamber. Cells were washed three times with PBS-Tween 0.1%. This was followed by a 1 h incubation with the secondary antibody goat anti-rabbit IgG H&L (Alexafluor 488) (Abcam ab150077). Caco-2 cells were washed three times with PBS-Tween 0.1%. The membrane of Transwell® inserts was removed and sealed using DAKO fluorescent mounting medium. Slides were analyzed with a confocal microscope Zeiss LSM 800 Airy-Scan (DImaCell platform, Besançon).

Staining of actin

Caco-2 cells were seeded in chamber-slide at 12,000 cells per well. After 2 h incubation with TB, NP200, NP30 at 10 mg mL^{-1}, Cyt B at 20 µg mL^{-1} or 22 h after recovery, Caco-2 cells were washed twice with PBS and then fixed with 3.7% paraformaldehyde during 15 min at room temperature. Cells were first permeabilized with 1% Triton X-100 during 10 min under gentle agitation. Actin was labelled with 150 nM Acti-stain 488 phalloidin (Cytoskeleton, Inc. PHDG1-A) for 45 min at room temperature in humid chamber. Cells were washed twice with PBS. This was followed by a 1 min-incubation with DAPI. Caco-2 cells were washed twice with PBS. The chamber-slide were sealed using DAKO fluorescescent mounting medium. Slides were analyzed with a confocal microscope Zeiss LSM 800 AiryScan (DImaCell platform, Besançon).

Statistics

All data are means ± SEM. Comparisons between the experimental groups and control were performed by one-way ANOVA analysis and the Holm Sidak test (Sigmastat software). A difference was considered significant at $p \leq 0.05$.

Results

Physicochemical properties of the nanoparticles

The physicochemical properties of silica NPs were determined in saline transport buffer (TB). The size was measured by dynamic light scattering and the zeta potential by laser Doppler electrophoresis. The physicochemical characterization of silica NPs was reported in Table 1. Mean size of NP200, NP70, NP30 and NP10 were respectively 215, 71, 32 and 20 nm. The additive E551 was characterized by a hydrodynamic diameter of 268 nm. PDI of E551 and NP10 was around 0.23 suggesting a wider size distribution compared to NP200, NP70 and NP30 which is less than 0.1. The zeta potential was around of − 20 mV for all silica particles including the E551.

Physicochemical characteristics of silica NPs were monitored for 2 h in TB to evaluate their physical stability for in vitro studies (Fig. 1). The hydrodynamic diameters and the size distributions were stable for all silica NPs.

Effect of nanoparticles on Caco-2 and co-culture Caco-2/HT29-MTX cell viability

Caco-2 and co-culture were exposed for 2 h to silica NPs at two concentrations in TB (1 and 10 mg mL^{-1}). The cell viability was then determined by MTT assay (Fig. 2a, b). For the two in vitro models, the viability stayed above

Table 1 Physicochemical properties of silica nanoparticles in transport buffer using a ZetaSizer

Silica NPs	Mean diameter (nm)	Polydispersity index	Zeta potential (mV)
NP200	215 ± 7	0.026 ± 0.15	− 21.3 ± 0.6
NP70	71 ± 4	0.018 ± 0.019	− 19.0 ± 2.6
NP30	32 ± 2	0.055 ± 0.031	− 17.7 ± 0.7
NP10	20 ± 6	0.236 ± 0.010	− 18.5 ± 1.1
E551	268 ± 19	0.231 ± 0.029	− 20.5 ± 0.6

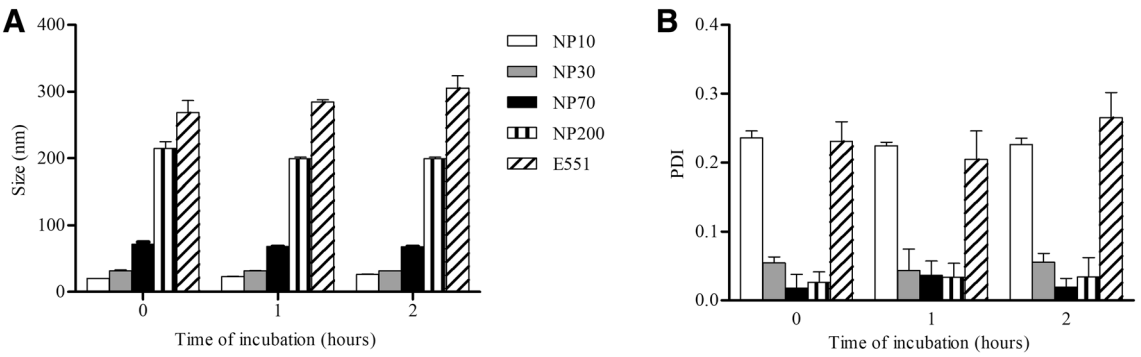

Fig. 1 Physical stability of silica nanoparticles at 1 mg mL^{-1} for 2 h in transport buffer at 37 °C. The mean diameter (**a**) and the polydispersity index (**b**) were measured on at least two different batches of silica NPs using a Zetasizer. Data are means ± SEM from triplicate

80%, suggesting the lack of cytotoxic effect of silica particles including E551. The cytotoxicity of silica NPs was also determined by measuring the LDH release (Fig. 2c, d). In Caco-2, E551, NP70 and NP30 at high concentration induced a light cytotoxicity of 7%, 14% and 15%, respectively, as compared to the control. Cytotoxicity of NP30 was not concentration-dependent with similar values at 1 and 10 mg mL^{-1}. The same results were obtained with the co-culture.

Effect of nanoparticles on the intestinal permeability

Caco-2 and co-culture were exposed to silica NPs for 2 h in TB and then, the permeability was monitored by transepithelial electrical resistance (TEER) measurement (Fig. 3a, b). In co-culture model, the smallest NPs including NP70, NP30 and NP10 at 10 mg mL^{-1} led to a TEER decrease comprised between 10 and 30% of the control. The TEER drop was exacerbated with the Caco-2 monolayer and especially in the presence of NP30. A TEER decrease of 27% and 61% was measured at 1 and 10 mg mL^{-1} of NP30, respectively. No effect of NP200 and E551 was obtained with the co-culture, whereas a TEER decrease of 9% and 20% was observed with E551 at 1 and 10 mg mL^{-1}, respectively, in Caco-2 monolayer.

The paracellular transport of LY through the Caco-2 monolayer and the co-culture was evaluated after 2 h incubation with silica NPs (Fig. 3c, d). NP30 and NP10 at 10 mg mL^{-1} facilitated the LY transport across the intestinal barrier in the two in vitro models. The apparent permeability was 1.5-fold higher in the co-culture compared with the control medium. No significant effect of NP200, NP70 and E551 was reported in both in vitro models.

Reversible effect of silica NPs on Caco-2 permeability

The TEER of the Caco-2 monolayer was monitored 22 h after 2 h exposure to NP30 at 10 mg mL^{-1} and Cyt B at 20 µg mL^{-1} (Fig. 3e). As previously observed, NP30 induced a significant TEER decrease. Cyt B also altered the

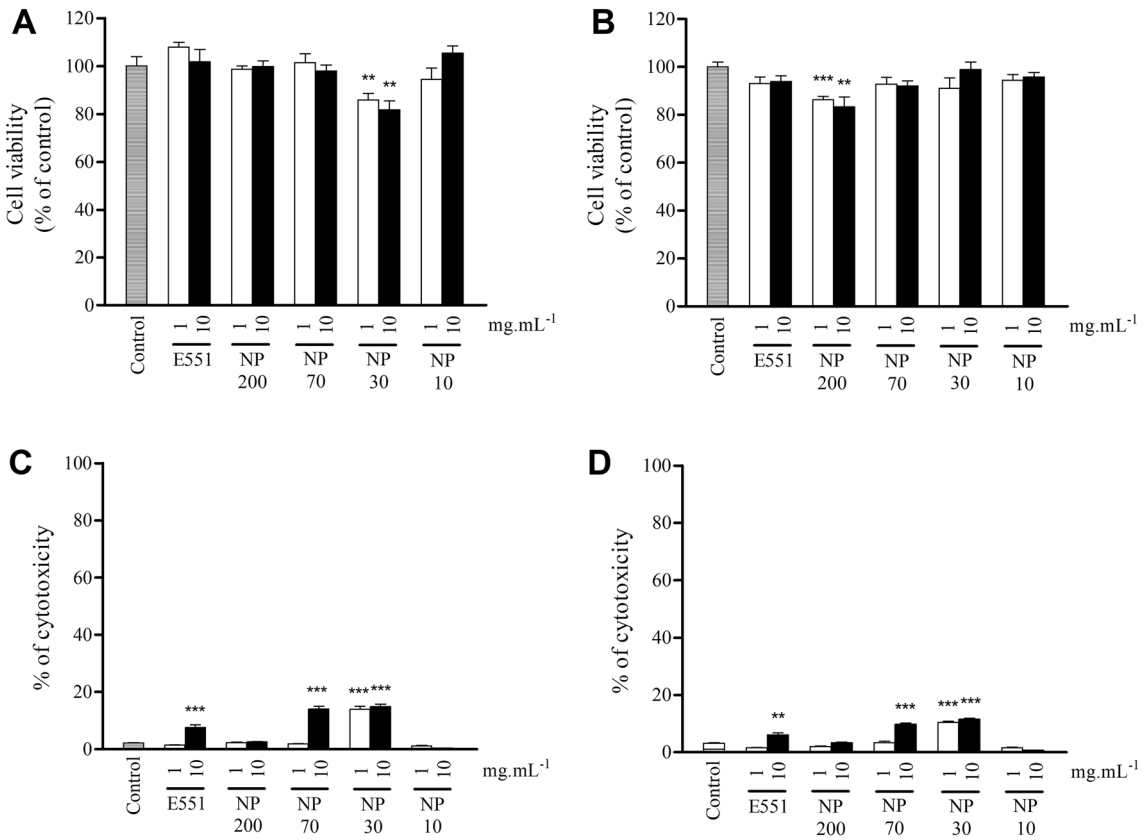

Fig. 2 Effect of the silica NPs (1 and 10 mg mL^{-1}) on cell viability in Caco-2 (**a**, **c**) and co-culture Caco-2/HT29-MTX (**b**, **d**) after 2 h exposure. Cell viability was determined by an MTT assay (**a**, **b**) and cytotoxicity was determined by an LDH assay (**c**, **d**). Results are expressed as percent of control medium (transport buffer without any NP) for cell viability assay. For LDH activity, results were expressed as % of cytotoxicity. Data are means ± SEM from triplicate of three independent cultures. $^{**}p \leq 0.01$ and $^{***}p \leq 0.001$ with respect to control

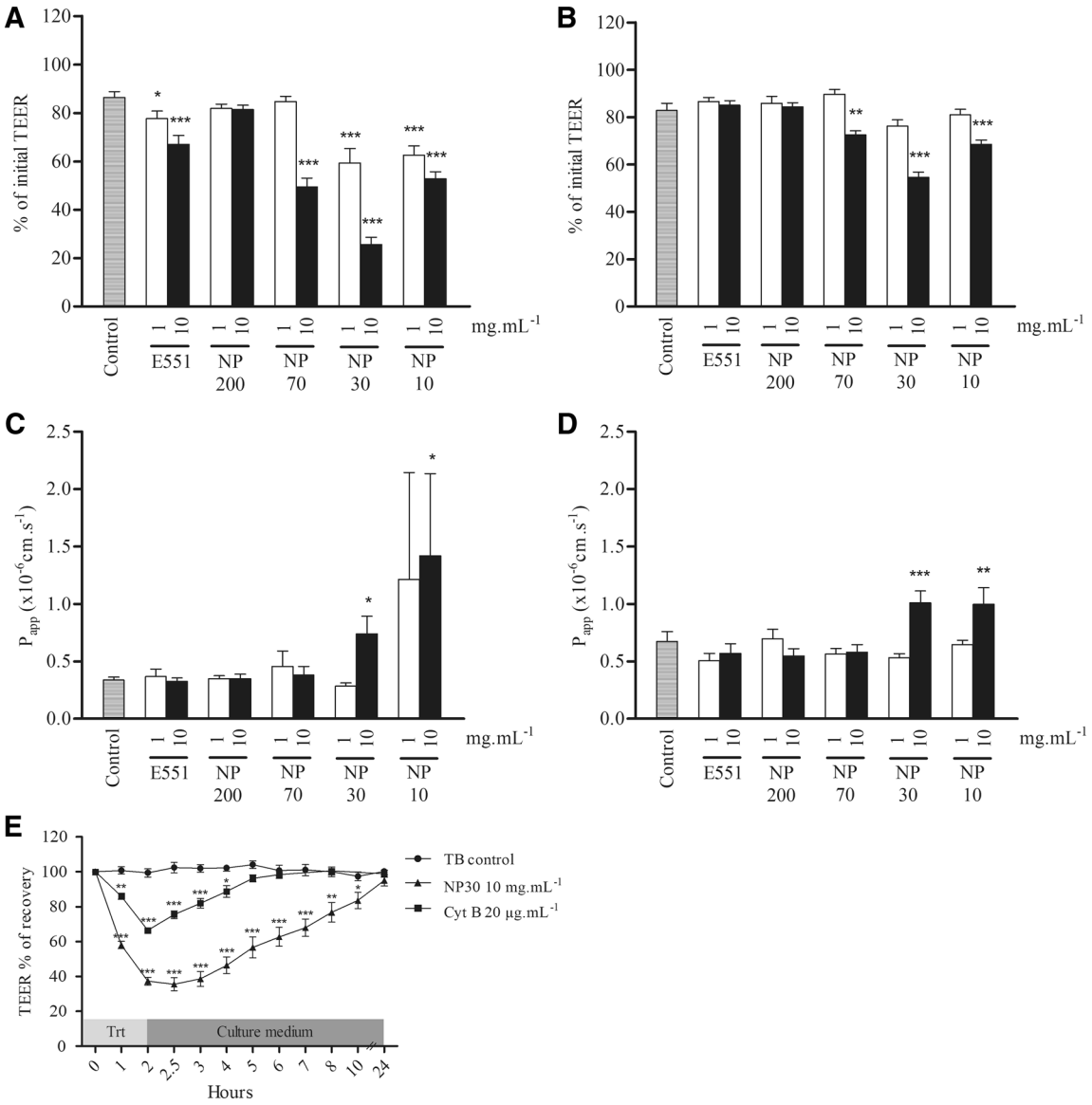

Fig. 3 Effect of the silica NPs (1 and 10 mg mL^{-1}) on cell permeability in Caco-2 (**a**, **c**) and co-culture Caco-2/HT29-MTX (B and D) after 2 h exposure. Cell permeability was determined by TEER measurement (**a**, **b**) and assessment of Lucifer-Yellow paracellular transport (**c**, **d**); data are means ± SEM from triplicate of at least four independent cultures. TEER monitoring of Caco-2 cells exposed to NP30 (10 mg mL^{-1}) and Cyt B (20 µg mL^{-1}). "Trt" means treatment (**e**); data are means ± SEM from duplicate of at least three independent cultures. $*p \leq 0.05$, $**p \leq 0.01$ and $***p \leq 0.001$ with respect to control

TEER values at a lower degree than NP30 at 10 mg mL^{-1} (34%). After Cyt B treatment, at least 4 h were necessary for a full TEER recovery. Regarding the NP30 treatment, TEER increased steadily over 22 h to finally reach the values of control.

Uptake of silica NPs in Caco-2 cells and co-culture

The uptake of silica NPs in Caco-2 cells was determined after 2 h exposure using fluorescent NPs (Fig. 4). At 37 °C, 71% of NP30 were taken up by Caco-2 cells versus 18% for the NP200 ($p \leq 0.01$). At 4 °C, only 4% of NP30 were adsorbed on Caco-2 cells as compared with 37 °C ($p \leq 0.001$), whereas no temperature effect was reported with NP200. The NP30 uptake in the co-culture was tremendously reduced compared to the Caco-2 monolayer with only 27% of detected particles ($p \leq 0.05$).

Cellular oxidative stress and inflammatory response induced by silica NPs

The cellular oxidative stress was determined by the quantification of ROS in Caco-2 and co-culture after incubation with

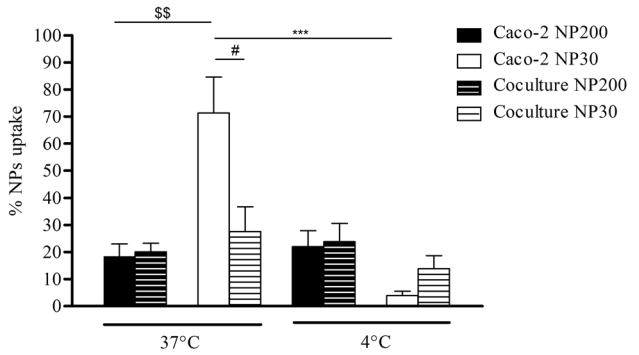

Fig. 4 Uptake of fluorescent silica NPs in Caco-2 cells or co-culture at 37 °C or 4 °C after 2 h exposure. Data are means ± SEM from triplicate of three independent cultures. $^{\#}p \leq 0.05$: Caco-2 30 nm at 37 °C compared to co-culture 30 nm at 37 °C. $^{\$\$}p \leq 0.01$: Caco-2 200 nm at 37 °C compared to Caco-2 30 nm at 37 °C. $^{***}p \leq 0.001$: Caco-2 30 nm at 37 °C compared to Caco-2 30 nm at 4 °C

silica NPs for 2 h in TB (Fig. 5a, b). Except for NP200, silica nanoparticles induced a ROS production in both in vitro models at 10 mg mL^{-1}. The increase of relative rate of ROS ranged between 1.5 and 2.1 in the Caco-2 monolayer. A similar effect was detected with the additive E551.

The secretion of IL-6 and IL-8 was also evaluated by ELISA assay (Fig. 5c–f). Only NP10 at 10 mg mL^{-1} significantly increased the IL-6 secretion in the Caco-2 monolayer and the co-culture. No secretion was measured for the other silica NPs except for NP30 at 1 mg mL^{-1} in Caco-2 model. Moreover, NP30 and NP10 induced a significant secretion of IL-8 at highest concentration in both models. The concentrations of pro-inflammatory cytokines including IL-6 and IL-8 were approximately two times higher with the Caco-2 monolayer compared with the co-culture. Release of IL-1α and IL-10 was also studied but not detected whatever the treatment (data not shown).

Effect of silica NPs on tight junctions

Tight junction proteins in Caco-2 cells previously exposed to silica NPs and Cyt B were quantified by western blotting (Fig. 6a, b). Actin was used as the reference protein and the control without any treatment was set at 1. The ZO-1 expression was similar to the control for all the treatments. Claudin 2 expression was unchanged with NP30 and NP200, as compared to the control medium.

The ZO-1 protein in the Caco-2 monolayer was also observed by confocal microscopy after 2 h incubation with silica NPs and Cyt B (Fig. 6c–e). A continuous staining of ZO-1 was observed after all the treatments. For each image, the width of fluorescent staining was measured at different points (Fig. 6i). Untreated cells were used as the control and set at 1. Fluorescent labeling width was increased by 1.3-fold after treatment with NP30 at 10 mg mL^{-1}. A 1.2-fold increase was reported with Cyt B. No significant effect of NP200 at 10 mg mL^{-1} on the labeling width was observed (data not shown). Twenty-two hours after the end of the treatments (Fig. 6f–h) corresponding to the time necessary to the full TEER recovery, the enlarging of ZO-1 staining bands was not observed anymore for NP30 and Cyt B with widths equal to 90% of control values. Expression of Claudin 2 was also studied by confocal microscopy (data not shown). No difference between control and silica NP treatment in the expression and the localization of this protein was noticed.

Effect of silica NPs on actin cytoskeleton

Actin cytoskeleton of Caco-2 cells was labeled and observed by confocal microscopy after treatments with silica NPs and Cyt B (Fig. 7). In contrast to NP200, NP30 at 10 mg mL^{-1} and Cyt B led to a total disruption of actin filaments after 2 h incubation. De novo actin filaments were identified 22 h after the end of the treatments.

Discussion

Silica NPs were physically stable in TB after 2 h incubation. This stability conferred by the negative surface charge of silica nanoparticles in TB allowed considering the size effect of NPs during the in vitro experiments. The high polydispersity index of the additive E551 suggests a wide size distribution of silica particles. The 2 h duration corresponds to the mean residence time of components administered by the oral route in the major absorbing segments of the small intestine including jejunum and ileum (Billat et al. 2017). NP30 and NP10 at 10 mg mL^{-1} increased the LY paracellular transport across the Caco-2 and Caco-2/HT29-MTX cultures after 2 h treatment. Silica NPs with sizes ranging between 10 and 70 nm induced a TEER drop in both in vitro models in a concentration- and size-dependent manner, whereas no effect was observed with NP200. The TEER values in the Caco-2 monolayer were around twofold lower with NP30 compared with NP10 and NP70, suggesting a target size in the modulation of the intestinal permeability. Additive E551 induced also a TEER decrease in the Caco-2 monolayer, while no effect was detected with the Caco-2/HT29-MTX model. In addition, the effects of NP30 on the TEER were significantly reduced with the co-culture, presumably due to the mucus layer as compared to the Caco-2 monolayer. This result was in accordance with the cell uptake studies which revealed a tremendous difference in the NP30 internalization between the two in vitro models. After 2 h exposure at 37 °C, 71% and 27% of NP30 added in the donor compartment were detected in the Caco-2 and Caco-2/HT29-MTX cultures, respectively. When incubation was performed at 4 °C, only

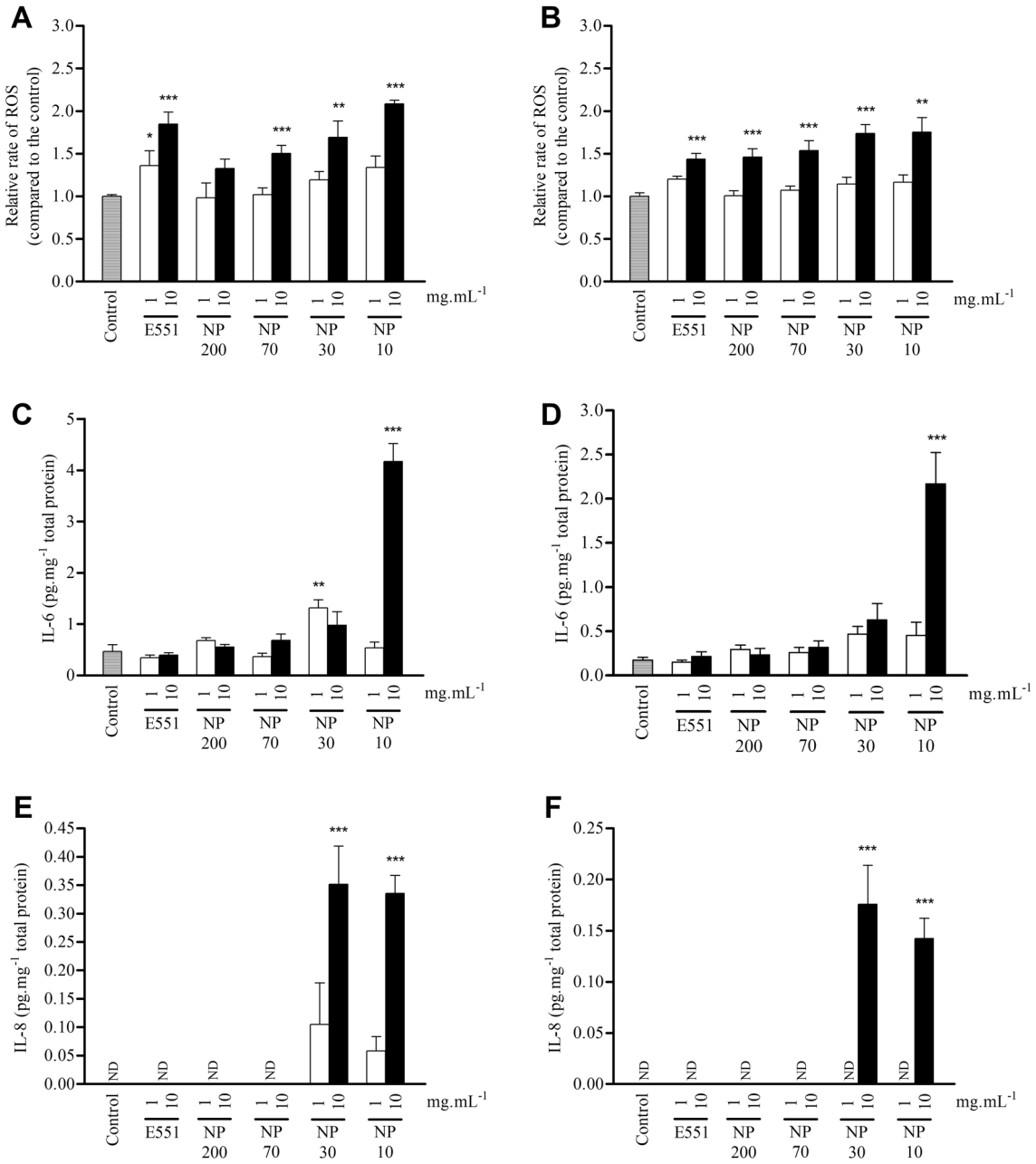

Fig. 5 Effect of the silica NPs (1 and 10 mg mL^{-1}) on ROS production in Caco-2 (**a**) and Caco-2/HT29-MTX co-culture (**b**) after 2 h exposure. Rate of ROS was expressed as versus control. IL-6 (**c**, **d**) and IL-8 (**e**, **f**) secretions were determined by ELISA assay after 2 h exposure of the silica NPs (1 and 10 $mg.mL^{-1}$) in Caco-2 model (**c**, **e**) or in co-culture (**d**, **f**). IL secretions were reported to the amount of total proteins. Data are means ± SEM from duplicate of three independent cultures. $*p \leq 0.05$, $**p \leq 0.01$ and $***p \leq 0.001$ with respect to control. *ND* non detectable

4% of NP30 were in contact with the Caco-2 monolayer, demonstrating the intracellular location of the majority of NP30 at 37 °C. These results emphasize the protective effect of mucus which reduces the accessibility of epithelial cells for the NP30, thus limiting the TEER drop. This was consistent with the permeability results observed with the additive E551. The large size distribution of the E551 suggests the presence of a few small particles which could affect in the same way the Caco-2 monolayer permeability. The effect was fully inhibited by the presence of the mucus in the co-culture. No mucus effect was detected with NP200 due to the lack of internalization in epithelial cells. This was consistent with previous findings that showed a low uptake of 150 nm silica NPs in Caco-2 cell-lines and could explain the lack of intestinal modulation with NP200 (Ye et al. 2017).

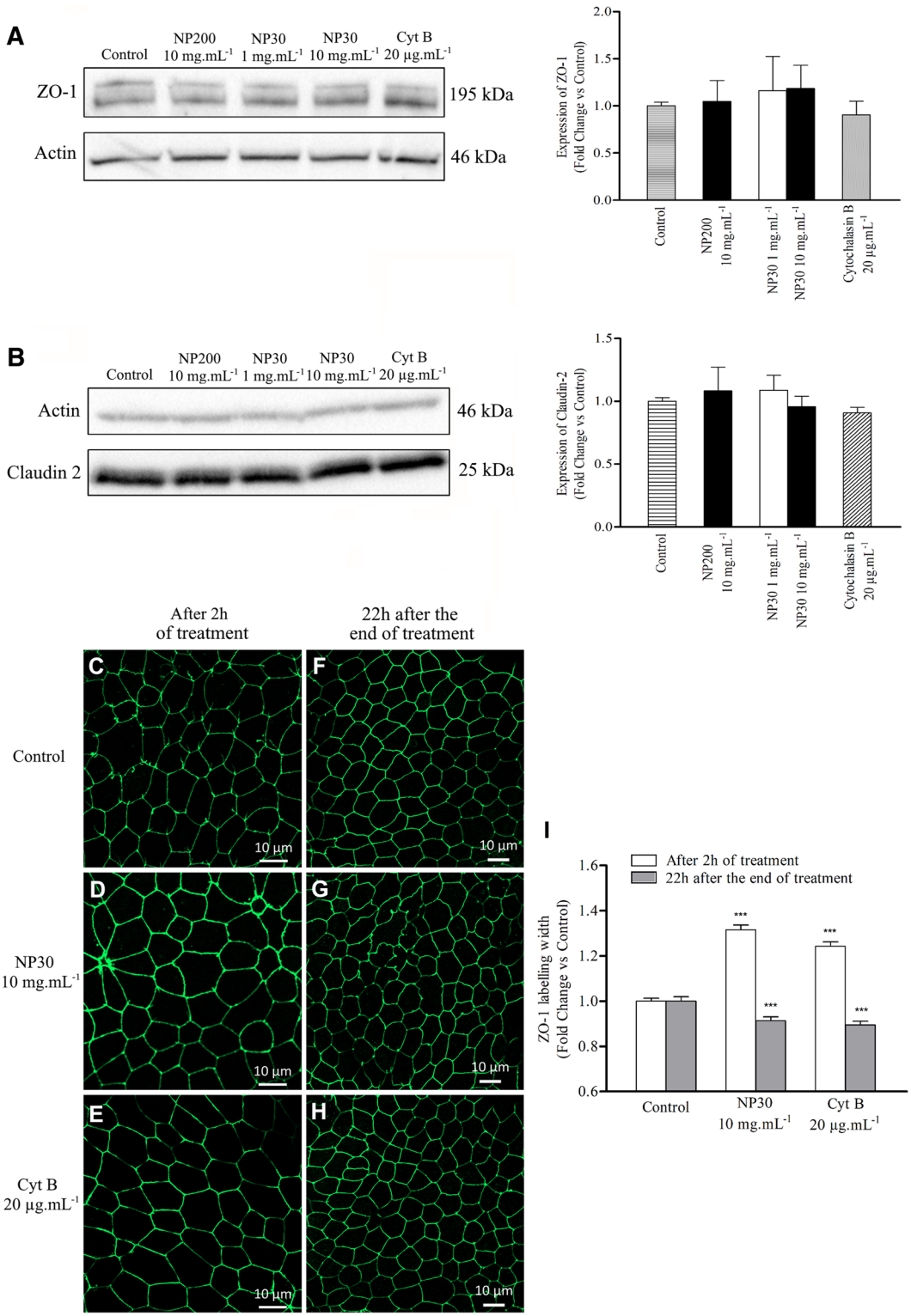

Fig. 6 Changes in relative expression of ZO-1 (**a**) and Claudin 2 (**b**) after 2 h exposure to silica NPs (10 mg mL^{-1}) or Cyt B (20 µg mL^{-1}) in Caco-2 cells. Data are means ± SEM from three independent cultures. ZO-1 immunostaining in Caco-2 cells after 2 h incubation with TB (**c**), NP30 (10 mg mL^{-1}) (**d**) and Cyt B (20 µg mL^{-1}) (**e**) or 22 h after the end of the treatment (**f**–**h**). Representative image of three independent cultures. ZO-1 labeling width (**i**) was expressed as versus control. Data are means ± SEM from at least 20 points per image of three independent cultures. *$p \leq 0.05$ and ***$p \leq 0.001$ with respect to control

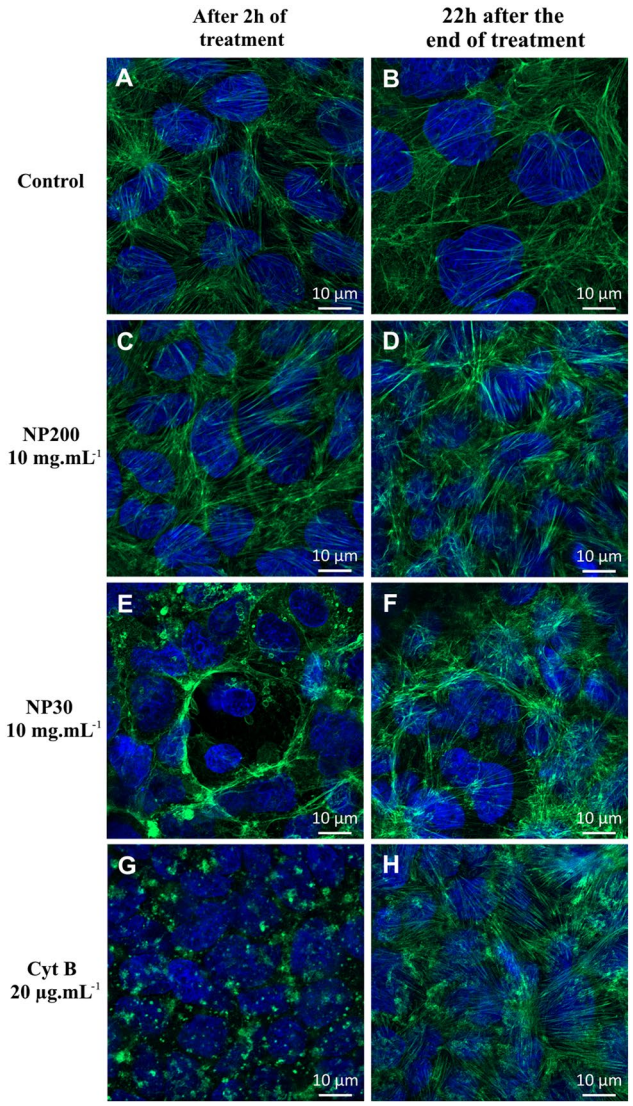

Fig. 7 Actin staining in Caco-2 cells after 2 h incubation with TB (**a**), NP200 (10 mg mL^{-1}) (**c**), NP30 (10 mg mL^{-1}) (**e**) and Cyt B (20 µg mL^{-1}) (**g**) and 22 h after the end of the treatment (**b**, **d**, **f**, **h**). Representative image of three independent cultures

NPs were incubated with epithelial cells at non-cytotoxic concentrations as demonstrated using two complementary studies. MTT assays revealed that at least 80% of cells were still viable after 2 h exposure. Additionally, the low LDH release observed with the Caco-2 monolayer after the NP30-incubation was not concentration-dependent in contrast to the permeability modulation. No LDH release was observed with NP10 whereas a TEER decrease was measured. In the lack of cytotoxic effects, modulation of paracellular permeability is often caused by a dysfunction of tight junctions (TJ) (Lemmer and Hamman 2013). TJ are composed of transmembrane proteins such as claudins, and occludins and cytoplasmic proteins (ZO-1, ZO-2 and ZO-3). The ZO protein ties the transmembrane proteins to actin cytoskeleton. This multiprotein network limits the intracellular space dimensions which do not exceed 50 Angstroms, preventing the passage of large compounds (Kirby and Linklater 2016). NPs can affect directly the TJ by modulating the intracellular signal transduction or indirectly by inducing oxidative stress and/or inflammation (Rao 2008; Lee 2015).

Li et al. showed that gold NPs characterized by a mean diameter of 150 nm modulated the blood–brain barrier permeability in mice (Li et al. 2015). By inhibiting the PKCζ protein kinase isoform, gold NPs reduced the threonine phosphorylation of occludin and ZO-1. Disassembly and degradation of TJ in endothelial cells were then observed. However, TJ protein downregulation was not observed with the same gold NPs in Caco-2 and HCT116 epithelial cells, suggesting a cell-dependent mechanism. This was consistent with our findings which revealed that ZO-1 and Claudin 2 expressions were not significantly affected after treatment with NP30 despite the paracellular permeability increase.

Oxidative stress was detected in both Caco-2 monolayer and co-culture in a concentration-dependent manner after 2 h incubation with the additive and all the nanoparticles. These findings were consistent with the work of Christen et al. which showed a ROS activity after incubation of silica NPs in human hepatoma cells (Christen et al. 2014). A relationship between the oxidative stress induced by NPs and the TJ dysfunction in the blood–brain barrier was reported (Liu et al. 2017). ROS including superoxide, hydrogen peroxide and hydroxyl radicals may disrupt either directly the ZO-1/occludin complex or indirectly after rearrangement of actin cytoskeleton due to protein modifications by thiol oxidation and tyrosine phosphorylation (Rao 2008). However, our results showed that the oxidative stress was not correlated with the permeability modulation. ROS activity levels were in the same range for all the tested NPs, while only NP30 followed by NP10 and NP70 induced a significant TEER drop.

Inflammatory response was observed in mono-and co-cultures after some NP treatments. Only NP10 induced the IL-6 release in the two in vitro models. Suzuku et al. showed that IL 6 increases the paracellular permeability of the intestinal epithelium by regulating the Claudin 2 expression involved in the well-known "pore" pathway of paracellular flux (Suzuki et al. 2011; Weber 2012). However, this mechanism does not explain the strong TEER drop induced by the NP30. By contrast, both NP10 and NP30 involved in the intestinal permeability modulations triggered the IL-8 release by epithelial cells in a concentration-dependent manner. No IL-8 was detected with the other sizes of NPs. The interleukin concentrations were two times higher in the Caco-2 monolayer compared with the co-culture, confirming the protective effect of mucus as previously discussed. IL-8 secretion by Caco-2 cell lines was also reported by Tarantini et al. after incubation of

silica nanoparticle when their size was 20 nm by transmission electron microscopy (TEM) and 53 nm by dynamic light scattering (DLS) (Tarantini et al. 2015). In the same study, no cytokine secretion was observed with silica NPs with a hydrodynamic diameter of 123 nm. IL-8 released from infected human dermal microvascular endothelial cell lines increased the paracellular transport across the monolayer. IL-8 was responsible for the disorganization of actin structures and the displacement of occludins in the cytoplasm (Talavera et al. 2004). However, in the present study, no modulation of the permeability of the Caco-2 monolayer was observed after addition of recombinant IL-8 (data not shown). This result disproves the hypothesis of a direct correlation between the inflammatory response and the intestinal permeability.

Considering that the oxidative stress and the inflammatory response were not directly corroborated with the enhanced permeability of the intestinal barrier, the direct interaction of NP30 on the actin cytoskeleton was investigated using only the Caco-2 cell lines, exhibiting a high TJ expression compared with the HT29-MTX (Kleiveland 2015). Many findings demonstrated the role of the actin cytoskeleton in the epithelial permeability (Rodgers and Fanning 2011) as well as the cytoskeleton disruption induced by NP cell uptake (Ispanixtlahuatl-Meráz et al. 2018). The NP30 effects were compared to Cyt B, a fungal toxin well known to disrupt the actin microfilaments and to increase the epithelial permeability (Ma et al. 2000). Interestingly, a permeability drop and a TEER recovery were observed after treatment with Cyt B at 20 µg mL^{-1} and NP30 at 10 mg mL^{-1}. The reversible effect of the cytochalasin D (Cyt D) on the permeability modulation of MDCK monolayers was previously reported by Stevenson et al. (1994). Disruption of actin microfilaments in Caco-2 cells was observed by confocal microscopy after NP30 and Cyt B treatments, while no effect was observed with NP200. Surprisingly, the expression of ZO-1 assessed by western blotting was not affected by both NP30 and Cyt B despite the paracellular permeability modulation. This finding was confirmed by immunofluorescence studies which showed a continuous labeling of ZO-1 at the cell surface. However, both NP30 in a concentration-dependent manner and Cyt B increased the width of the ZO-1 band compared with the "no treatment" control and the NP200. The band enlarging was not visible anymore 22 h after the treatments, corresponding to the time necessary to the complete TEER recovery. This observation suggests a relaxation of TJ network due to the anchorage loss with the actin cytoskeleton and may explain the intestinal permeability increase. The hypothesis was supported by Van Itallie et al. who stated ZO-1 stabilizes the tight junction barrier by coupling to the perijunctionnal actin (Van Itallie et al. 2009). In addition, Madara et al. demonstrated that the filamentous structure condensation in the presence of Cyt D induced the widening of spaces between enterocytes and increased the intestinal permeability (Madara et al. 1986, 1987).

Conclusion

In conclusion, silica NPs exposed to in vitro models of intestinal barrier induced oxidative stress as well as an inflammatory response for the smallest NPs. A size- and concentration-dependent modulation of the intestinal permeability was observed in presence of NPs in both in vitro models. The highest modulation was observed with small NPs, especially NP30. E551 additive also decreased the TEER values in the Caco-2 monolayer. The large size distribution of the food additive suggests the presence of a small NP ratio which could affect the intestinal permeability. By limiting the cell internalization of small silica NPs, mucus reduced even prevented in the case of the E551, the TEER drop in the co-culture. In addition, pro-inflammatory cytokine secretion and oxidative stress were also lower in the co-culture. Thus, the protective role of mucus has to take into account for a relevant estimation of the oral nanotoxicity. TEER recovery was obtained within 22 h following the treatment, suggesting a reversible effect of NPs. The increase of the intestinal permeability by the NPs was explained by the disruption of the actin cytoskeleton, altering the ZO-actin binding involved in the stability of TJ network. This hypothesis was supported by the enlarging of ZO-1 bands, suggesting the dilatation of spaces between epithelial cells as well as by the concomitant recovery of actin filaments and TEER values. In addition, no modification of Claudin 2 and ZO-1 expressions was observed, discarding the hypothesis of a TJ dysregulation. This work emphasizes the potential risk of small silica NPs administered by the oral route.

Acknowledgements Raphaël Cornu is supported by a fellowship from the "Communauté d'Agglomération du Grand Besançon (CAGB)". We thank DImaCell microscopy facilities, especially M. Tissot for her technical assistance (Plateforme DImaCell, Univ. Bourgogne Franche-Comté, F-25000 Besançon, France). The authors thank FHU InCREASe for the Oral Communication Award and the financial support.

Compliance with ethical standards

Conflict of interest The authors declare that they have no conflicts of interest.

References

Athinarayanan J, Periasamy VS, Alsaif MA et al (2014) Presence of nanosilica (E551) in commercial food products: TNF-mediated oxidative stress and altered cell cycle progression in human

lung fibroblast cells. Cell Biol Toxicol 30:89–100. https://doi.org/10.1007/s10565-014-9271-8
Barahona F, Ojea-Jimenez I, Geiss O et al (2016) Multimethod approach for the detection and characterisation of food-grade synthetic amorphous silica nanoparticles. J Chromatogr A 1432:92–100. https://doi.org/10.1016/j.chroma.2015.12.058
Billat P-A, Roger E, Faure S, Lagarce F (2017) Models for drug absorption from the small intestine: where are we and where are we going? Drug Discov Today 22:761–775. https://doi.org/10.1016/j.drudis.2017.01.007
Brun E, Barreau F, Veronesi G et al (2014) Titanium dioxide nanoparticle impact and translocation through ex vivo, in vivo and in vitro gut epithelia. Part Fibre Toxicol 11:13. https://doi.org/10.1186/1743-8977-11-13
Christen V, Camenzind M, Fent K (2014) Silica nanoparticles induce endoplasmic reticulum stress response, oxidative stress and activate the mitogen-activated protein kinase (MAPK) signaling pathway. Toxicol Rep 1:1143–1151. https://doi.org/10.1016/j.toxrep.2014.10.023
EFSA Panel on Food Additivies, and Nutrient Sources added to Food (ANS), Younes M, Aggett P et al (2018) Re-evaluation of silicon dioxide (E 551) as a food additive. EFSA J. https://doi.org/10.2903/j.efsa.2018.5088
He X, Deng H, Hwang H (2019) The current application of nanotechnology in food and agriculture. J Food Drug Anal 27:1–21. https://doi.org/10.1016/j.jfda.2018.12.002
Ispanixtlahuatl-Meráz O, Schins RPF, Chirino YI (2018) Cell type specific cytoskeleton disruption induced by engineered nanoparticles. Environ Sci Nano 5:228–245. https://doi.org/10.1039/C7EN00704C
Jackson TC, Patani BO, Israel MB (2017) Nanomaterials and cell interactions: a review. JBNB 08:220–228. https://doi.org/10.4236/jbnb.2017.84015
Kirby R, Linklater AKJ (eds) (2016) Monitoring and intervention for the critically ill small animal: the rule of 20. Wiley Blackwell, Ames
Kleiveland CR (2015) Co-cultivation of Caco-2 and HT-29MTX. In: Verhoeckx K, Cotter P, López-Expósito I, et al. (eds) The impact of food bioactives on health: in vitro and ex vivo models. Springer International Publishing, Cham, pp 135–140
Lee SH (2015) Intestinal permeability regulation by tight junction: implication on inflammatory bowel diseases. Intest Res 13:11–18. https://doi.org/10.5217/ir.2015.13.1.11
Lemmer HJR, Hamman JH (2013) Paracellular drug absorption enhancement through tight junction modulation. Expert Opin Drug Deliv 10:103–114. https://doi.org/10.1517/17425247.2013.745509
Li C-H, Shyu M-K, Jhan C et al (2015) Gold nanoparticles increase endothelial paracellular permeability by altering components of endothelial tight junctions, and increase blood–brain barrier permeability in mice. Toxicol Sci 148:192–203. https://doi.org/10.1093/toxsci/kfv176
Liu X, Sui B, Sun J (2017) Blood-brain barrier dysfunction induced by silica NPs in vitro and in vivo: Involvement of oxidative stress and Rho-kinase/JNK signaling pathways. Biomaterials 121:64–82. https://doi.org/10.1016/j.biomaterials.2017.01.006
Ma TY, Hoa NT, Tran DD et al (2000) Cytochalasin B modulation of Caco-2 tight junction barrier: role of myosin light chain kinase. Am J Physiol 279:G875–G885. https://doi.org/10.1152/ajpgi.2000.279.5.G875
Madara JL, Barenberg D, Carlson S (1986) Effects of cytochalasin D on occluding junctions of intestinal absorptive cells: further evidence that the cytoskeleton may influence paracellular permeability and junctional charge selectivity. J Cell Biol 102:2125–2136. https://doi.org/10.1083/jcb.102.6.2125
Madara JL, Moore R, Carlson S (1987) Alteration of intestinal tight junction structure and permeability by cytoskeletal contraction. Am J Physiol 253:C854–861. https://doi.org/10.1152/ajpcell.1987.253.6.C854
Pedata P, Ricci G, Malorni L et al (2019) In vitro intestinal epithelium responses to titanium dioxide nanoparticles. Food Res Int 119:634–642. https://doi.org/10.1016/j.foodres.2018.10.041
Pradhan N, Singh S, Ojha N et al (2015) Facets of nanotechnology as seen in food processing, packaging, and preservation industry. Biomed Res Int 2015:1–17. https://doi.org/10.1155/2015/365672
Rao R (2008) Oxidative stress-induced disruption of epithelial and endothelial tight junctions. Front Biosci 13:7210–7226
Rodgers LS, Fanning AS (2011) Regulation of epithelial permeability by the actin cytoskeleton. Cytoskeleton 68:653–660. https://doi.org/10.1002/cm.20547
Sahu SC, Hayes AW (2017) Toxicity of nanomaterials found in human environment: a literature review. Toxicol Res Appl. https://doi.org/10.1177/2397847317726352
Stevenson BR, Begg DA (1994) Concentration-dependent effects of cytochalasin D on tight junctions and actin filaments in MDCK epithelial cells. J Cell Sci 107(Pt 3):367–375
Suzuki T, Yoshinaga N, Tanabe S (2011) Interleukin-6 (IL-6) regulates claudin-2 expression and tight junction permeability in intestinal epithelium. J Biol Chem 286:31263–31271. https://doi.org/10.1074/jbc.M111.238147
Talavera D, Castillo AM, Dominguez MC et al (2004) IL8 release, tight junction and cytoskeleton dynamic reorganization conducive to permeability increase are induced by dengue virus infection of microvascular endothelial monolayers. J Gen Virol 85:1801–1813. https://doi.org/10.1099/vir.0.19652-0
Tarantini A, Lanceleur R, Mourot A et al (2015) Toxicity, genotoxicity and proinflammatory effects of amorphous nanosilica in the human intestinal Caco-2 cell line. Toxicol In Vitro 29:398–407. https://doi.org/10.1016/j.tiv.2014.10.023
Van Itallie CM, Fanning AS, Bridges A, Anderson JM (2009) ZO-1 stabilizes the tight junction solute barrier through coupling to the perijunctional cytoskeleton. Mol Biol Cell 20:3930–3940. https://doi.org/10.1091/mbc.e09-04-0320
Vancamelbeke M, Vermeire S (2017) The intestinal barrier: a fundamental role in health and disease. Expert Rev Gastroenterol Hepatol 11:821–834. https://doi.org/10.1080/17474124.2017.1343143
Weber CR (2012) Dynamic properties of the tight junction barrier: dynamic properties of the tight junction barrier. Ann N Y Acad Sci 1257:77–84. https://doi.org/10.1111/j.1749-6632.2012.06528.x
Ye D, Bramini M, Hristov DR et al (2017) Low uptake of silica nanoparticles in Caco-2 intestinal epithelial barriers. Beilstein J Nanotechnol 8:1396–1406. https://doi.org/10.3762/bjnano.8.141
Zhou Y, Quan G, Wu Q et al (2018) Mesoporous silica nanoparticles for drug and gene delivery. Acta Pharmaceut Sin B 8:165–177. https://doi.org/10.1016/j.apsb.2018.01.007